NASA TM-88829

NASA Technical Memorandum 88829

Advanced Optical Measuring Systems for Measuring the Properties of Fluids and Structures

Arthur J. Decker
Lewis Research Center
Cleveland, Ohio

Prepared for the
Symposium on Propulsion Instrumentation
cosponsored by the National Aeronautics and Space Administration and
the Chinese Aeronautical Establishment
Jiangyou, People's Republic of China, October 6–10, 1986

NASA

ADVANCED OPTICAL MEASURING SYSTEMS FOR MEASURING

THE PROPERTIES OF FLUIDS AND STRUCTURES

Arthur J. Decker
National Aeronautics and Space Administration
Lewis Research Center
Cleveland, Ohio 44135

SUMMARY

Four advanced optical methods are reviewed for the measurement or visualization of flow and structural properties. Double-exposure, diffuse-illumination, holographic interferometry can be used for three-dimensional flow visualization. When this method is combined with optical heterodyning, precise measurements of structural displacements or fluid density are possible. Time-average holography is well known as a method for displaying vibrational mode shapes, but it also can be used for flow visualization and flow measurements. Deflectometry is used to measure or visualize the deflection of light rays from collimation. Said deflection occurs because of refraction in a fluid or because of reflection from a tilted surface. The moire technique for deflectometry, when combined with optical heterodyning, permits very precise measurements of these quantities. The rainbow schlieren method of deflectometry allows varying deflection angles to be encoded with colors for visualization.

INTRODUCTION

For more than 40 years, NASA Lewis Research Center has used interferometry (Mach-Zehnder interferometry, for example) and deflectometry (Töpler Schlieren, for example) for measuring and visualizing flow properties (refs. 1 and 2). The invention of the laser in 1960 (ref. 3) made it practical to use interferometry for structural measurements as well (ref. 4). In fact, since the early 1970's, most research and development in optical instrumentation at Lewis has involved laser optics. Both laser velocimetry and laser spectroscopy (refs. 5 to 10) have become important, along with laser interferometry and laser deflectometry. The effort in laser spectroscopy is new at Lewis. Laser velocimetry is being reviewed in another presentation by A. Strazisar. This presentation is a review of interferometry and deflectometry. A history of the use of these methods at Lewis is summarized by figure 1.

Figure 1 shows the importance of laser optics for the period, 1972 to the present. Only the rainbow schlieren (ref. 11), among instrument systems actually developed during that period, does not use laser illumination. Very reliable continuous wave lasers such as the helium-neon laser and the argon-ion laser could be purchased commercially beginning in the early 1970's. The development of reliable, commercially available, pulsed lasers required more time (ref. 12). Good ruby lasers could be purchased by the mid 1970's and reliable Nd:YAG lasers became available about 1979. Since 1979, other laser technologies have become available enough to be considered for applications to interferometry and deflectometry. Among these lasers are various dye lasers, the copper vapor laser, and the alexandrite laser. Our approach at Lewis is to use commercially available lasers for propulsion experiments. Sometimes, a slightly modified version of the laser is purchased to insure that the special

requirements of a laser for holographic interfer- ometry are met, including both spatial and temporal coherence.

Keeping in mind this brief discussion of how we acquire our lasers, the remainder of this review will emphasize four of the techniques shown in figure 1. The four are: double-exposure, diffuse-illumination, holographic interferometry; time-average holographic interferometry; moire deflectometry; and rainbow schlieren. This author has been involved extensively with the first two techniques (refs. 13 to 17). He has worked cooperatively with a National Research Council Associate from Israel on the third technique (ref. 18). The fourth technique, rainbow schlieren, has been developed exclu- sively by a colleague of the author (ref. 11), and is a good example of how one can make significant contributions to simple, nonlaser, optical instruments for propulsion research.

The remainder of this review begins by discussing the structural and flow properties that can be measured or visualized using holographic interferometry and deflectometry. These properties are also summarized by figure 1. Then diffuse-illumination, double-exposure, holographic interferometry is reviewed as a flow visualization technique for visualizing large density gradients. The next step discussed is to combine diffuse-illumination interferometry with optical heterodyning. Very precise measurements of the displacement of a structural surface are then possible. The projections of fluid-density changes can also be measured precisely and automatically. Optical heterodyning has been used in interferometry since 1969 (refs. 19 to 21), but the availability of inexpensive computers and computer-controlled accessories has made it especially attractive, recently. Next, time-average holography is reviewed, not only for its application to vibrational analysis, but also for its appli- cation to flow visualization. The two examples of deflectometry are reviewed next. Moire deflectometry permits projections of the gradient of density to be measured. Laser moire deflectometry can be used with optical heterodyning for precise, automated measurements (refs. 18 and 22 to 24). Rainbow schlieren requires a very simple modification of the Töpler schlieren system (ref. 11). Flow visualization and the measurement of light-ray refraction in a fluid are thereby improved. The rainbow schlieren also uses white-light illumination, unlike the other methods which require a laser.

HOLOGRAPHIC INTERFEROMETRY

Holography

Laser holography most often implies the use of the off-axis-reference- wave technique, originally proposed by Leith and Upatnieks (ref. 25). The implementation of this technique is discussed extensively in books and papers (refs. 26 and 27). The author's experiences with holographic techniques are summarized briefly, before the application to interferometry is discussed.

A person can learn quickly to record very good holograms of small, simple objects. For that purpose, as in figure 2, it is convenient to have: a small vibration isolation table; a helium-neon laser which radiates at least 5 mW; a high-resolution, silver-halide emulsion on film or glass plates (Kodak SO253 or Agfa-Gevaert 10E75 emulsion for low power helium-neon lasers, for example); a glass-plate or film holder; two microscope-objective, spatial-filter combi- nations; a selection of mirrors or prisms; a variable density beam splitter;

and film processing. A student can learn to record excellent holograms with that equipment.

By contrast, as shown in figure 3, it is often very difficult or expensive to record good holograms of complex subjects such as propulsion flows (ref. 28). The limitations on recording holograms of propulsion flows include: the need to use a pulsed laser; test-rig vibrations and motions; poor or difficult optical access; reflections from components such as windows; extreme temperature variations; electrical interference; dust and oils; the need for remote control; and, at times, inadequate or unreliable lasers and hologram recording materials.

Nevertheless, the objectives are the same for both simple and complex subjects. The primary objective is to record and to reconstruct a light wave having the exact, relative, time-independent phase of the light wave from the laser-illuminated scene. This objective is to be accomplished, while minimizing extraneous waves or noise and while using the full linear dynamic range of the recording material for maximum brightness or efficiency.

The primary objective can be stated in a different and more useful form, provided that the geometrical optics approximation is valid. That approximation must be valid, in any case, for measuring the macroscopic variables of interest in aeronautics. Then, the objective of holography is to record and to reconstruct light rays, where each light ray is characterized by a positionally dependent, relative phase (eikonal) (ref. 29), given by

$$\phi = \frac{2\pi}{\lambda} G \int_{S_1}^{S_2} \rho(r) \, dS \qquad (1)$$

where λ is the wavelength of the laser beam, G is the Gladstone-Dale coefficient (G = 0.227×10^{-3} m³/kg for air at λ = 532 nm), $\rho(r)$ is the density of the fluid through which the light ray passes, r is a position on the light ray, and S is distance along the light ray.

Once an acceptable hologram is recorded, the hologram becomes irrelevant to the concept of the measurement process, except as an aperture in the optical measurement system. The objective is to use interferometry to measure the light-ray phase ϕ.

Interferometry

There is a major difference between classical interferometry (Mach-Zehnder interferometry, for example) and holographic interferometry. Classical interferometry compares the instantaneous state of an object with an external reference (ref. 2); whereas, holographic interferometry compares one state of a fluid or structure with another. The result is a cosine interference-fringe pattern

3

$$I = I_1 + I_2 \cos(\Delta\phi) \tag{2}$$

where

$$\Delta\phi = \phi_2 - \phi_1 \tag{3}$$

is the difference in phase along the light ray (the interference phase) between the two states of the object. Figure 4 shows a cosine interference-fringe pattern corresponding to the difference between bent and unbent states of a cantilever beam. Holographic interferometry is used to measure precisely relative changes in a fluid or structure. In principle, a complete history of a time-varying fluid or structure can be recorded by using a high enough hologram recording rate.

Holographic interferometry itself is discussed thoroughly by Vest (ref. 30). The three common implementations are real-time, double-exposure, and time-average holographic interferometry. In real-time holographic interferometry, the wave from the actual object interferes with the reconstructed wave from a hologram of another state of the object. This technique requires good mechanical stability of the apparatus and is usually confined to the laboratory. In double-exposure holography, typically two holograms of different states of the object are recorded by the same photographic emulsion. The two waves are reconstructed simultaneously and interfere. This implementation of holographic interferometry is the most versatile. Time-average interferometry compares a continuum of states of an object with one another, where each state is effectively weighted by the time the state is occupied. Time-average holography seems to be the oldest useful application of holographic interferometry, and is used for vibrational analysis.

Irrespective of which form of interferometry is used, there are three ways that the phase in equation (1) can change, and each is potentially interesting in aeronautics. They are: a change in the length $S_2 - S_1$ of a light ray, resulting from the deflection of a structure from which the light ray is reflected; a change in fluid density $\rho(r)$; and a change in the anomalous refractive index in the neighborhood of an optical resonance. Only the first two will be discussed.

One assumption, always made, is that interference is between corresponding light rays. That is, the geometry of the light ray is assumed to change negligibly between the states compared. That assumption may be incorrect, if there are large structural motions or large changes in refraction between states. In diffuse-illumination, holographic interferometry, high-contrast interference fringes cannot be formed unless the assumption is valid.

Two other important assumptions are that the fringe pattern is formed either from density changes only or from structural changes only. A combination of the two changes is difficult to interpret. Referring to figure 5, the change in phase due to structural motion is then given by

$$\Delta\phi(r) = \frac{4\pi}{\lambda} \frac{(\vec{k}_i - \vec{k}_r)}{2} \cdot \vec{\delta}(r) \tag{4}$$

4

where $\vec{k}_i$ is a unit vector along the ray direction of incidence, $\vec{k}_r$ is a unit vector along the ray direction of reflection, and $\vec{\delta}(r)$ is the displacement of the structure at the point of reflection. The vector $\vec{k}_i - \vec{k}_r/2$ is sometimes called the sensitivity vector.

The following points should be kept in mind.

(1) Three measurements, requiring three different light rays, are required at each point to determine the three components of the displacement. Diffuse-illumination interferometry, in principle, allows one hologram to be used for the three measurements.

(2) The quantities of structural importance involve derivatives of the displacement field. If δ_x and δ_y represent in-plane components of displacement, and δ_z represents the normal component of displacement, then the following quantities can be determined (refs. 20 and 31).

Three of the six independent components of strain,

$$\epsilon_{xx} = \frac{\partial \delta_x}{\partial x} \tag{5}$$

$$\epsilon_{yy} = \frac{\partial \delta_y}{\partial y} \tag{6}$$

$$\epsilon_{xy} = \epsilon_{yx} = \frac{1}{2}\left(\frac{\partial \delta_x}{\partial y} + \frac{\partial \delta_y}{\partial x}\right) \tag{7}$$

Bending along direction α relative to the local x-axis,

$$\Delta K\alpha = \frac{\partial^2 \delta_z}{\partial x^2}\cos^2\alpha + 2\frac{\partial^2 \delta_z}{\partial x \partial y}\cos\alpha\,\sin\alpha + \frac{\partial^2 \delta_z}{\partial y^2}\sin^2\alpha \tag{8}$$

Torsion along direction α relative to the local x-axis,

$$\frac{d\Omega}{dS} = \frac{\partial^2 \delta_z}{\partial x \partial y}\cos^2\alpha + \frac{1}{2}\left(\frac{\partial^2 \delta_z}{\partial y^2} - \frac{\partial^2 \delta_z}{\partial x^2}\right)\sin^2\alpha \tag{9}$$

The equations for bending and torsion neglect certain strain dependent terms (refs. 20 and 31).

(3) The quantities above can be determined locally by numerical differentiation (ref. 20) of the measured displacements or by fitting the displacement field with spline functions (ref. 30). Numerical differentiation requires that the fringe pattern be measured very accurately, and a heterodyne or quasi-heterodyne fringe measurement method (ref. 21) must be used.

The change in phase due to a density change $\Delta\rho(r)$ is given by

$$\Delta\phi = \frac{2\pi}{\lambda} G \int_{S_1}^{S_2} \Delta\rho(r) \, dS \tag{10}$$

The determination of $\Delta\rho(r)$ from measurements of $\Delta\phi$ requires, in general, a 180° field of view and the use of the techniques of computed tomography (ref. 32). Smaller fields of view can be used if additional information is supplied to the calculational procedure. The simplest case is the two-dimensional approximation, where

$$\Delta\rho(r) = \Delta\rho(x,y) \tag{11}$$

and a single view is adequate. The following points should be kept in mind.

(1) The light ray may exhibit significant curvature or refraction (refs. 2 and 33). Most calculations based on equation (10) assume a refractionless limit.

(2) The inversion procedures for obtaining $\Delta\rho(r)$ use the derivatives of $\Delta\phi$ (spatial derivatives of the fringe pattern) or related quantities (ref. 32). Heterodyne or quasiheterodyne fringe measurement methods are desirable for accuracy (ref. 18).

(3) The field of view is usually much less than 180°, especially for internal propulsion flows. Restricted-field-of-view tomography is required.

(4) Holographic interferometry yields the absolute density only when one state of the flow is a no-flow or quiescent condition.

This section is concluded with the following comments. So far, interference has been computed between two different states of a fluid or structure, within a single light ray. In diffuse-illumination, holographic interferometry, each point in the cosine interference fringe pattern, equation (2), actually involves imaging a pencil or cone of light rays as shown in figure 6. A high-contrast fringe pattern can be imaged only when the variation of $\Delta\phi$ is negligible over that pencil or cone. This requirement is a so-called fringe localization condition, and will be reviewed in the section on double-exposure, diffuse-illumination, holographic interferometry.

Deflectometry, reviewed in the next section, is used to measure the deflection of a light ray from a collimated condition

DEFLECTOMETRY

Light rays are deflected from collimation, when they are reflected from a tilted surface or when they are refracted. The case of refraction is the important case at Lewis.

Refraction of a light ray, by air, for example, is caused by a component of the gradient of the refractive index or density perpendicular to the light ray. The refraction angles in the xz and yz planes, respectively, for

6

light initially collimated parallel to the z axis, approximately satisfy the equations

$$\theta_x(x, y) = G \int_{Z_1}^{Z_2} \frac{\partial \rho}{\partial x} \, dz \tag{12}$$

$$\theta_y(x, y) = G \int_{Z_1}^{Z_2} \frac{\partial \rho}{\partial y} \, dz \tag{13}$$

where, again, G is the Gladstone-Dale coefficient relating changes in refractive index to changes in fluid density.

The techniques for visualizing or measuring (θ_x, θ_y) can be divided roughly into two categories: those based on spatial filtering (ref. 34) of the Fraunhofer diffraction pattern of a flow (Töpler and rainbow schlieren, for example) (refs. 1 and 11) and those based on Fresnel diffraction by the actual instrument (shadowgraphy and moire, for example) (refs. 35 to 37).

Interferometry is sometimes compared with deflectometry to determine which technique is the most desirable for a particular application. The following five general advantages of deflectometry can be kept in mind when making a comparison:

(1) Deflectometry is conceptually simple, involving the filtering or encoding of light rays as a function of deflection angle.

(2) Deflectometry has adjustable sensitivity. The sensitivity of a Töpler schlieren can be changed by changing the focal length of the decollimating lens or mirror.

(3) Deflectometry is generally less costly than the various forms of interferometry.

(4) Deflectometry uses white-light sources for most applications.

(5) Deflectometry detects the derivatives of the light-ray phase, equation (1), directly. The measurements should be better conditioned for performing computed tomography.

The advantages are balanced by the following five disadvantages:

(1) Deflectometry requires very good mirrors, windows, and lenses; since, refractions and decollimations by the optical components are also detected.

(2) Deflectometry has a field of view determined by the diameter of the optical system. Consequently, a large field of view requires large windows, mirrors, or lenses.

(3) Deflectometry provides a single view, perspective, or projection of the flow field. The measurement of three-dimensional flows requires multiple views.

7

(4) Deflectometers, especially schlieren systems, are difficult to calibrate for quantitative applications, particularly if a photographic step is involved.

(5) Deflectometers based on moire require laser illumination for best performance and sensitivity, thereby cancelling the white-light advantage.

The remainder of this report reviews four measurement methods based on holographic interferometry or deflectometry.

DOUBLE-EXPOSURE, DIFFUSE-ILLUMINATION, HOLOGRAPHIC INTERFEROMETRY

Advantages and Disadvantages

Double-exposure, diffuse-illumination, holographic interferometry can be considered to be the principal representative of holographic interferometry. A sample interferogram is shown in figure 4. The technique has many potentially useful properties:

(1) Multiple views or perspectives are reconstructable from the same hologram. In fact, diffuse illumination is required to realize holography's three-dimensional imaging property. In principle, one hologram can be used to determine three components (δ_x, δ_y, δ_z) of a displacement field or to determine the density-change field $\Delta\rho(r)$ (ref. 30).

(2) The interference-fringe pattern is localized. That is, high contrast interference fringes are formed by a camera, only when it is focused on certain points in the reconstructed image. This property can be used for three-dimensional flow visualization (refs. 14 to 16), if certain requirements are met.

(3) The time between exposures can be made small enough to record interferograms of objects that are varying rapidly as a function of time. In principle, a time history of a subject can be measured with interferometric precision. Holographic cinematography is potentially useful (ref. 38).

(4) Two distinct reference beams, one for each exposure, can be used. During reconstruction, the frequency of one beam can be shifted relative to that of the other, thereby allowing the fringe pattern to be measured by means of optical heterodyning.

Unfortunately, these advantageous properties are compromised by some serious disadvantages:

(1) There is a laser speckle effect (ref. 39). Intensity varies rapidly on a scale of the order of the resolution of the imaging system used to view the reconstruction. An average local intensity can be defined reliably only if a large detector is used to average over many speckles. Similarly, large detectors are needed to make reliable phase measurements, when optical heterodyning is required.

(2) Fringe contrast is degraded by real or apparent (refraction induced) motion of the system diffuser (ref. 28). Some real or apparent motion of the system diffuser will always occur between exposures. Transverse motion equal

to one resolution element (objective speckle diameter) will eliminate fringes, entirely.

(3) Since diffuse illumination is inefficient, larger lasers may be required. Spurious reflections may overwhelm the useful diffuse illumination.

(4) In structural analysis, the fringes may not localize on the structure, requiring the application of a projection theorem and resulting in reduced positional accuracy.

(5) The large intensity variations of the laser speckle effect increase the nonlinear noise problems of holography.

Some of these disadvantages, particularly 2 and 3, make it more difficult to use holography in a propulsion environment.

Fringe Localization and Flow Visualization

In diffuse-illumination interferometry, reflection from or transmission through a diffuser as in figure 6 adds a random term to the time-independent phase of equation (1). Consequently, there is no definite interference between different light rays. Interference between exposures, as given by equations (4) and (10), must occur within the same light ray. A picturesque viewpoint is to imagine that the individual light rays are strings. The diameter of a string is equal to the overall resolution of the viewing system. A string must not change shape between exposures so much that it does not overlap its former self to some extent. Technically speaking, the speckle patterns of the two reconstructions must be correlated.

The interference pattern in diffuse-illumination, double-exposure, holographic interferometry is formed by a lens as in figure 6. The lens sums individual light rays at the imaged point, so that the intensity at the point is given by

$$I \propto \sum_i I_{1i} + \sum_i I_{2i} \cos(\Delta\phi_i) \tag{14}$$

The fringe pattern will have high contrast, only for those images of points where the variation of $\Delta\phi_i$ is negligible within the imaging pencil or cone. Otherwise, the cosine terms in equation (14) will cancel. A first-order criterion for high contrast is the fringe localization condition:

$$\frac{\partial \Delta\phi}{\partial\theta_{ix}} = 0 \tag{15}$$

$$\frac{\partial \Delta\phi}{\partial\theta_{iy}} = 0 \tag{16}$$

where θ_{ix} and θ_{iy} are angles about the central ray z in the xz and yz planes, respectively (fig. 6).

9

An example of the fringe localization effect is shown in figure 7. The figure shows two photographs of the fringe pattern of a flame-induced flow over a cascade blade. In the left photograph, the camera was focused on the blade tip. The fringe pattern to the right of the blade is out of focus and shows low contrast. For the right-hand photograph, the camera was focused for maximum fringe contrast. The reconstructed image of the blade tip is seen to be out of focus. Maximum fringe contrast for the fringes at the right or suction surface of the blade occurred when the camera was focused at midspan. That plane is the surface of localization for those fringes.

The fringe localization effect has been applied primarily to three-dimensional visualization of time-varying shock wave surfaces (refs. 14 to 16, and 40). Time variation occurs because the shock wave is moving, because the shock wave is changing shape, or because the strength of the shock wave is changing. One technique (rapid-double-exposure technique) for visualizing shock waves uses two exposures which are very close together. For transonic compressors, the time between exposures is of the order of microseconds. It is presumed meaningful to talk about an average shock-wave surface. The fringe pattern will localize on or nearby that shock-wave surface, if one or more of the following conditions are true (ref. 14).

(1) The view is confined to within ±10° of tangency to the shock-wave surface.

(2) The curvature of the shock wave is large.

(3) The strength of the shock wave changes substantially between exposures.

(4) The strength of a moving shock wave varies substantially as a function of position on the shock-wave surface.

The author does not wish to underestimate the difficulties of using this technique, which are listed below:

(1) The calculation of the curve or surface of localization can be complex (refs. 14 and 16).

(2) The fringe contrast is easily degraded by many factors (ref. 28). For example, more than 10 percent difference in exposure energies seriously reduces contrast.

(3) For shock waves, the fringes may localize far enough away from the shock-wave surface to produce a large fringe-localization error. One of the fringe-localization conditions summarized above must hold strongly to avoid this problem.

Nevertheless, very good results have been achieved at times. Figure 8 shows fringes formed by the shock waves in a transonic flutter cascade, where forced-blade vibrations resulted in time-varying lambda shock waves. Figure 9 is a photograph of the cascade itself. The back sidewall of the cascade is diffusely reflecting. The light from a frequency doubled, Q-switched, double-pulsed, Nd:YAG laser is admitted through the window, where it is reflected from the back sidewall and passes through the flow passage and out the same window.

The visualization of the fringe patterns provides qualitative and positional information. The measurement of the fringe patterns is required to determine displacements and densities. A very accurate method for measuring fringe patterns is discussed next.

Heterodyne Diffuse-Illumination Interferometry

A localized fringe pattern has the form of equation (2) in double-exposure, diffuse-illumination interferometry. The objective is to determine $\Delta\phi$ from the pattern. Any attempt to determine $\Delta\phi$ from the intensity itself presents several problems:

(1) The sign of $\Delta\phi$ cannot be determined.

(2) Variations in intensity I caused by variations in I_1 and I_2 cannot be distinguished from variations in I caused by variations in $\Delta\phi$. Variations in I_1 and I_2, in turn, are caused by variations in illumination, coherence, correlation, polarization, and other factors not related to the interference phase $\Delta\phi$.

(3) The sensitivity of $\Delta\phi$ to changes in I is not constant. The sensitivity is largest near fringe minima and maxima.

The consequence of problems 2 and 3 is that intensity interferometry consists largely of identifying the positions of fringe maxima or minima. The interference phase $\Delta\phi$ is assigned integer values of π at these points, and is estimated in between by using interpolation functions. The problems with this approach are:

(1) Unless finite fringe interferometry can be used, there may be very few fringes, and consequently very few measurements.

(2) Interpolation will fail to show anomalies in structural and flow properties.

(3) The accuracy of the measurements, especially in the presence of laser speckle, may not be adequate to allow local differentiation of the data.

Referring to problem 3, the most straightforward way to estimate structural properties at a point is to differentiate numerically the displacement distribution. Also, computed tomography for $\Delta\rho(r)$ requires derivatives and differences of the fringe pattern. The measurements must be very accurate to compute adequate derivatives of the fringe pattern.

Optical heterodyning is an answer to all the problems stated, although the technique generates its own problems. In optical heterodyning, a person starts with or creates a periodically time-varying light pattern, given most generally by

$$I = \sum_m I_m(r)\cos\{m[\omega t + \phi_I(r) + \phi_B(r)]\} \tag{17}$$

11

Where $\omega/2\pi$ is the fundamental frequency of the pattern, m is an integer, $\phi_I(r)$ represents an intelligence such as an interference phase, $\phi_B(r)$ is a bias, and $I_m(r)$ is a coefficient.

Conceptually, heterodyning works as follows. The time-varying intensity I is detected by a photodetector, and the signal is mixed with (multiplied by) a local oscillator signal at frequency $\omega/2\pi$. This process is responsible for the term "heterodyning." Simultaneously, the phase ϕ_I is measured relative to that of the local oscillator signal plus the bias ϕ_B. Such measurements can be made very accurately, independently of the coefficients I_m.

The simplest application of optical heterodyning is to interferometry, and that application has been performed since 1969 (ref. 19). The time-varying light pattern (fringe pattern) has the very simple form

$$I = I_1 + I_2\cos(\omega t + \Delta\phi) \tag{18}$$

where there is no bias. To first approximation, the accuracy of measuring $\Delta\phi$ does not depend on I_1, I_2, or the value of $\Delta\phi$, and the measurement can be performed at any position and for any value of $\Delta\phi$. The measurement is also sensitive to the sign of $\Delta\phi$.

Dändliker and his colleagues have studied the application of optical heterodyning to holographic interferometry, since about 1973 (refs. 20 and 21). The time-varying interference-fringe pattern of equation (18) is obtained with an apparatus, such as that shown schematically in figure 10. The object shown in that figure is a phase object called a flow simulator. It is used to evaluate or calibrate interferometers and deflectometers, and will be discussed later. Double-exposure holograms are recorded, where the state of the object changes between exposures. Two reference beams are used, one for each exposure of the double-exposure hologram. During the reconstruction step only, both reference beams are used, and the frequency of one reference beam is shifted relative to that of the other. An acoustooptic frequency shifter is used for this purpose. This step creates the time-varying fringe pattern of equation (18). A lens is used to form an image of the fringe pattern. Two detectors are used to detect the fringe pattern. For example, the detectors can be optical fibers routed to photomultiplier tubes. One detector is used as the reference for the other detector. The reference detector is fixed in position and is used to provide the equivalent of the local oscillator signal. The other detector is moved to different positions in the fringe pattern, where the measurements are made. The measurement then is really the difference in interference phase between two points in the fringe pattern. The measurement of relative interference phase is actually accomplished using a phase meter. The two detector signals are inputs to the phase meter, and the heterodyne process is accomplished automatically. One kind of phase meter is a dual-phase lock-in amplifier.

Dändliker has demonstrated phase-measurement accuracies of 0.4° for structural, diffuse-illumination interferograms (ref. 20). The equivalent in intensity-measurement interferometry is the ability to distinguish a change in the position of a fringe maximum of about 1/1000 fringe spacing.

The problems with heterodyne, diffuse-illumination interferometry are:

(1) There are random phase-measurement errors, related to misalignment of the processed hologram relative to the two reference beams (refs. 20 and 21). These errors can be incorporated into a single decorrelation coefficient γ, where no error corresponds to $\gamma = 1$. The error is given by

$$\delta\phi = \left[\frac{(1 - \gamma^2)}{2\gamma^2(N + 1)} \right]^{1/2} \tag{19}$$

where N is the number of speckles within the detector aperture. The sensitivity of γ to misalignment can be reduced by decreasing the angle between the reference beams.

(2) Large detectors (about 1 mm in diam) are required. The coefficient γ almost certainly will be less than unity, so that N, and consequently, the detector diameter must be large to compensate.

(3) There are systematic errors caused by misalignment of the processed hologram relative to the reference beams. These errors are minimized by keeping the imaging lens shown in figure 10 in contact with the hologram.

(4) There are systematic errors caused by the nonlinearities of the hologram recording process. These errors are minimized by keeping all objects, except for the object of interest, outside the field of view.

The approach to these problems at Lewis is to have careful alignment procedures in the laboratory, and to use a comparison or calibration object in the field. This calibration object, called a flow simulator, can also be used to demonstrate the performance of heterodyne, diffuse-illumination interferometry.

The flow simulator, figure 11, is a large crystal of KD*P (ref. 41). The crystal has 50 by 50 mm faces, which are perpendicular to the optic axis and are separated by 30 mm. Electrodes are attached to the 50 by 50 mm faces at four parallel edges. The two parallel 30 by 50 mm faces are accessible through windows for allowing light to pass through the crystal. Light polarized perpendicular to the optic axis experiences refractive index changes when voltages are applied to the electrodes. The double-exposure holograms compare voltage and no-voltage conditions.

Figure 12 shows sample interferograms for this crystal for various voltages on electrodes 2 and 4 (electrodes 1 and 3 grounded). The laser illumination has passed through a diffuser before entering the crystal. The fringe patterns are quite sparse. Their measurement is a good demonstration of the heterodyne technique.

Figure 13 (ref. 18) shows results for the 5 kV condition of figure 12. The data represents measurements along a scan midway between the electrode faces. First the data was converted to refractive-index changes assuming the two-dimensional approximation. Then, the data was differentiated numerically. Recall that the derivative is a better test of the measurement process. Central differences were used, where the data points were separated by 1 mm. Also included for comparison are predicted error ranges, corresponding to several

postulated fringe measurement accuracies. An uncertainty less that ±1/300 fringe is required to yield the results shown in the figure.

Because the change of state of the crystal can be repeated precisely, the crystal is a suitable object for calibrating or checking heterodyne, diffuse-illumination interferometry in a wind tunnel, for example.

This section is concluded with some additional comments:

(1) In the laboratory, heterodyne, diffuse-illumination interferometry requires a large continuous-wave laser such as an argon-ion laser, to obtain a large enough signal.

(2) There is a quasiheterodyne technique, where the relative phase, rather than the frequency, of the two reference beams is shifted (ref. 21). The intensities, corresponding to at least three different phase shifts at a point in the fringe pattern, can be used to determine the interference phase.

(3) Another major incentive for using heterodyne or quasiheterodyne techniques is that they can be automated using inexpensive computers and computer controlled hardware.

Another (and to some more familiar) form of holographic interferometry is time-average holographic interferometry. That technique is reviewed next for both structural and flow-properties measurements.

TIME-AVERAGE HOLOGRAPHY

Structures

If an object imparts a time-varying term $\phi(r,t)$ to the phase, and if a hologram is recorded of that object wave for an exposure-time T, then the linear recording property of holography assures that (refs. 42 and 43) the reconstructed object wave is proportional to

$$M = \frac{1}{T} \int_0^T \exp[j\phi(r,t)] \, dt \qquad (20)$$

where r refers to a diffuser coordinate for the light ray.

That is, the reconstruction is proportional to a time-average of the time-varying phase factor. The quantity defined by equation (20) has become known as the characteristic function. It has a simple interpretation only when the spatial and time variations of ϕ can be separated:

$$\phi(r,t) = \phi_r(r)\phi_t(t) \qquad (21)$$

The fact that the spatial and time coordinates of an object vibrating in a resonant, normal, characteristic, or eigen mode can be separated, led Powell and Stetson (ref. 4) to the first, and still one of the most useful, applications of continuous-wave-laser holographic interferometry: holographic vibrational analysis.

The displacement field of an object vibrating in a normal mode is given by the time-varying function

$$\vec{\delta}(r,t) = \vec{\delta}(r)\cos(\omega t + \beta) \tag{22}$$

where $\vec{\delta}(r)$ is now the displacement amplitude. From figure 5 and equation (4), the characteristic function becomes

$$M = \frac{1}{T} \int_0^T \exp j \; \frac{4\pi}{\lambda} \; \frac{(\vec{k}_1 - \vec{k}_r)}{2} \cdot \vec{\delta}(r)\cos(\omega t + \beta) \; dt \tag{23}$$

If the exposure time T is large compared with $2\pi/\omega$ or if T is exactly one cycle long, then

$$M = J_0 \left[\frac{4\pi}{\lambda} \; \frac{(\vec{k}_1 - \vec{k}_r)}{2} \cdot \vec{\delta}(r) \right] \tag{24}$$

This characteristic function is the well known Bessel fringe pattern of holographic vibrational analysis. For nonzero $\vec{\delta}$, the fringes depend on the sensitivity vector, but the display of the nodes of vibration ($\vec{\delta} = 0$) is unaffected by the sensitivity vector. A definitive display of the mode shapes of a structure is always possible. Figure 14 shows some mode shapes for a small blade.

Lewis has performed holographic vibrational analysis routinely since the early 1970's, using speckle interferometry (ref. 47) or real-time holographic interferometry to identify modes. This application of holographic interferometry is relatively easy to perform, although some care must be exercised, for example, to distinguish coupled modes from normal modes.

Flows

The application of time-average holography to flow visualization is not as well known as the application of time-average holography to vibrational analysis (ref. 15). The fringe-localization effect turns out to be the same for time-average, diffuse-illumination interferometry as for double-exposure, diffuse-illumination interferometry. The origin of this fact is easy to show.

For a time-varying density, equation (1) becomes

$$\phi(t) = \frac{2\pi}{\lambda} \; G \int_{S_1}^{S_2} \rho(r,t) \; dS \tag{25}$$

For short enough times t, the time coordinate can be separated from other coordinates because

$$\rho(r,t) \approx \rho_0(r) + \rho_0'(r)t \tag{26}$$

15

where ρ_0 is the density at $t = 0$, and ρ_0' is the time derivative of
the density at $t = 0$. The characteristic function is a function of the light
ray, and is obtained by substituting equations (25) and (26) in equation (20).
For a particular light ray passing through the fluid,

$$M = \exp[jA]\ \frac{\sin(A)}{A} \tag{27}$$

where

$$A = \frac{\pi G}{\lambda} \int_{S_1}^{S_2} T\rho_0'(r)\ dS \tag{28}$$

and where r refers to a position on the light ray. (Another pair of coor-
dinates can be used to define a light ray, but these coordinates have not been
explicitly shown here or elsewhere in this paper.)

But, for a small enough exposure time T,

$$\Delta\rho(r) = \rho_0'(r)T \tag{29}$$

With this approximation, the argument of M is exactly one-half the phase
difference $\Delta\phi$ of double-exposure holography as given by equation (10).
Hence,

$$M = \exp \frac{j\ \Delta\phi}{2}\ \sin \frac{\frac{\Delta\phi}{2}}{\frac{\Delta\phi}{2}} \tag{30}$$

The fringe-localization criterion in time-average holography is that M must
be constant to first order within the imaging pencil of figure 6. Hence, the
fringe-localization condition is again given by equations (15) and (16), since
M depends on $\Delta\phi$.

The photograph in figure 15 shows the fringe pattern from a time-average
hologram of a flow-induced flow over the same blade used for the double-
exposure hologram of figure 7.

The following three comments may be useful:

(1) The principal advantage of time-average holography for flow visuali-
zation is that the fringe contrast depends on $\Delta\phi$. By shifting the frequency
of the reference beam, the high-contrast fringe can be made to coincide with
the flow feature of interest (ref. 15), thereby enhancing its visualization.

(2) The sensitivity of time-average holography is one-half that of double
exposure holography. In double-exposure holography, the first dark fringe
requires that $\Delta\phi = \pi$. In time-average holography, the first dark fringe
requires that $\Delta\phi = 2\pi$.

(3) For time-varying, transonic flows, the exposure is typically measured
in tens of microseconds.

The laser also makes it possible to perform deflectometry quantitatively. Moire deflectometry is presented as an example, next.

MOIRE DEFLECTOMETRY

Moire deflectometry is an enticingly simple technique (refs. 35 to 37). Its use with optical heterodyning has been studied by Josef Stricker (refs. 22 to 24) in cooperation with the author (ref. 18).

Moire deflectometry allows the components of light-ray deflection, equations (12) and (13), to be measured independently. This measurement can be accomplished more precisely by using heterodyne moire deflectometry. The following review refers to the diagrams in figure 16.

One form of moire deflectometry requires the use of two coarse, rectangular-lined, diffraction gratings called Ronchi gratings, having typically 10 lines/mm. If the gratings are placed in contact, with their lines at a small relative angle θ, and if the pair is illuminated with collimated light, then the shadow or Fresnel diffraction pattern shows the familiar moire fringes. As in figure 16(b), if a pair of grating lines, one absorbing and the other transmitting, have a total width or pitch p, then the separation between moire fringes is given by

$$p' = \frac{p}{\theta} \tag{31}$$

If the gratings, called G_1 and G_2 in figure 16(a), are separated, but kept parallel, the pattern of moire fringes will persist. This pattern will have high contrast, if laser illumination is used and the gratings are separated by an integer multiple of p^2/λ, the so called Fourier image distance.

The key feature of moire deflectometry is that a deflection of a light ray, perpendicular to the bisector of the grating lines, causes a proportional deflection of the moire fringe pattern. If the bisector is directed along the y axis, as shown in figure 16(b), then a light-ray deflection component θ_x, given by equation (12) for example, will cause a moire-fringe shift given by

$$\delta h_y = \frac{\Delta}{\theta} \theta_x \tag{32}$$

where Δ is the separation between gratings.

The sensitivity is adjustable, as is the case with all deflectometry, and is proportional to the grating separation Δ. The sensitivity does not depend on the grating line-pitch p, but the spatial resolution of the instrument does. The reason is that the moire pattern is a spatial average of the Fresnel diffraction pattern or shadow of the grating pair. The average is evaluated over the pitch p.

Moire also offers a way to perform optical heterodyning. If one of the two gratings is translated at a constant speed V, with line angle θ constant, then the moire pattern will vary periodically at a fundamental frequency

$$\frac{\omega}{2\pi} = \frac{V}{p} \tag{33}$$

The actual time-varying pattern has the more general form of equation (17) and is approximately given by (ref. 18)

$$I \alpha \ \frac{1}{4} + \frac{2}{\pi^2} \sum_{m=0}^{\infty} \frac{\cos\left[\pi(2_{m+1})^2 \ \Delta^*\right]}{(2_{m+1})^2} \cos\left[2\pi(2_{m+1})\left(\frac{\omega t}{2\pi} + \frac{\theta x \Delta}{p} + \frac{Y\theta}{p} + \frac{x}{p}\right)\right] \tag{34}$$

where θ_x again is the deflection angle, and figure 16(a) shows the coordinates. Δ^* is the separation between gratings in Fourier image units.

Relating equation (34) to equation (17), the intelligence is given by

$$\phi_I = 2\pi \ \frac{\theta_x \Delta}{p} \tag{35}$$

and the bias is given by

$$\phi_B = 2\pi \left(\frac{Y\theta}{p} + \frac{x}{p}\right) \tag{36}$$

The parameter x is determined by the initial relative x position of the grating lines.

Conceptually, the heterodyne measurement is accomplished by filtering everything but the first harmonic (m=0), and then by measuring the phase of that harmonic relative to a reference. If the reference is derived from a second detector at an undeflected point in the moire pattern at the same value of y, then the bias is cancelled, yielding $2\pi \ \theta_x\Delta/p$ directly.

In practice, the grating speed is not constant. One grating is attached to an electromagnetic shaker or vibrator, as in figure 16(a). Two detectors are used, where one serves as a reference, and their outputs are transmitted to a phase meter. The phase meter is gated to the vibrator or shaker, so that measurements are made only during one direction of travel of the grating.

The analysis of the effects of this kind of motion is somewhat complex, but the consequences are easy to state. The transfer function of the phase measurement process becomes nonlinear. That is, the phase-meter reading is not linearly related to the deflection angle of the light ray. A calibration procedure is required (ref. 18). Nevertheless, the results that have been achieved are very encouraging.

Figure 17 (ref. 18) shows a comparison of heterodyne holographic interferometry with heterodyne moire deflectometry. The subject for the measurements was the flow simulator. The result for heterodyne holographic interferometry has already been presented as the lower part of figure 13.

The result for heterodyne moire shows more scatter than the result for heterodyne holography, but the same detailed features (peaks and valleys) are present in both plots in figure 17. The comparison is favorable, considering

18

that moire used the electromechanical modulation method and required a calibration procedure.

This section is concluded with the following comments:

(1) Moire deflectometry can be used, wherever there is a Töpler Schlieren system. Holography requires its own optical setup.

(2) Moire is limited by the general restrictions already listed for deflectometry.

(3) Moire can be performed with incoherent (white-light) illumination to some extent and requires lower-power lasers than holography, in any case.

Another form of deflectometry, rainbow schlieren, uses white-light sources exclusively. This technique, the final one reviewed, is the subject of the next section.

RAINBOW SCHLIEREN

The Howes rainbow schlieren (refs. 11 and 45 to 46) is an example of how, with some ingenuity, the performance of an old instrument can be improved. The rainbow schlieren, moire deflectometry, and a technique called local-reference-beam interferometry (ref. 47) are all readily incorporated into existing Töpler schlieren systems.

In the classic Töpler schlieren, the light from a small (point) light source is collimated by a lens or mirror. The light passes through a test section (flow), where it may be refracted according to equations (12) and (13). Then, a decollimating lens or mirror converges the light to its back focal plane, where an image of the light source is formed. Refracted rays are displaced from the optical axis in this plane, with the distance of displacement from the optical axis given by

$$d_x = f\theta_x \qquad (37)$$

$$d_y = f\theta_y \qquad (38)$$

where θ_x and θ_x are the deflection angles given by equations (12) and (13), and where f is the focal length of the decollimator.

If monochromatic light were used, modern Fourier optics terminology (ref. 34) would refer to the correspondence between (d_x, d_y) and (θ_x, θ_y), contained in the irradiance distribution in the back focal plane, as the angular or spatial spectrum. Any operation on the back-plane irradiance distribution would be called spatial filtering.

After spatial filtering in schlieren, a camera is used to form an image of the test section. Figure 18 (ref. 11) shows schematically the stated operations for a rainbow filter, although any other filter could be inserted.

The objective of filtering is to encode the refraction as variations of irradiance in the final image. The simplest approach is to use neutral density filters, where the half-plane filter or knife edge of Töpler schlieren is

the best known example. The quantitative information that can be determined by using a neutral density filter is very limited (ref. 11), and such filters are useful mainly for flow visualization.

Another approach is to use a color filter, consisting typically of three concentric rings, each transmitting a distinct color (ref. 48). Such discrete-color filters permit a significant increase in the information available from schlieren. The symmetry of the filter permits all directions of refraction to be visualized, and there are three angle-ranges measurable. (In fact, there are four, since rays that miss the filter will produce black, if the filter is in an absorbing holder.)

However, the abrupt changes between color zones cause diffraction by the filter, and the three colors yield little information for quantitative purposes. The rainbow filter improves on both of these difficulties.

The rainbow filter is also a concentric-ring filter, but the color or hue varies continuously as a function of radial position. The manufacturing process for the filter (ref. 46) begins by dispersing white light with a slit, diffraction-grating combination. The narrow spectrum is imaged onto a piece of film, which, in turn, is spun during exposure, thereby creating the circularly symmetrical filter. Either red or blue can be near the spin axis. The best performance is achieved by having a clear center and by having red at the edge of the filter. The diameter of the clear center is large enough to pass the image of the white-light source to show those regions of the flow that cause no refraction. This arrangement allows the full spectrum to be used for quantifying refraction: minimum measurable refraction angles are colored blue, and maximum measurable refraction angles are colored red. The filter is set in a black background, so that highly refracted rays that miss the filter produce black.

The actual size of the filter depends on the maximum value of $f\theta$. The desired filter is produced photographically as a reduced-size image of a master, which is manufactured as stated above (refs. 11 and 46).

Color photography is needed to show the actual performance of a rainbow schlieren, and reference 11 is highly recommended for this purpose. However, figure 19 is an enlarged black and white photograph of a rainbow filter. Figure 20 is another black and white print of a rainbow-schlieren photograph of cooling plates, and figure 21 shows the relative refractive-index distributions measured at four positions of the cooling plates. The measurements required that the colors be identified using an optical comparator.

Rainbow schlieren has been used for visualization; to quantify symmetrical flows; and for measuring properties of turbulence (ref. 11).

Before concluding this review, it is mentioned that deflectometry is diffraction-limited, and that there are different diffraction-limitations imposed by different components in the deflectometer (including the flow, ref. 11). The diffraction limits are quite different for intensity and heterodyne detection (ref. 24). By contrast, diffuse-illumination interferometry is shot-noise limited (ref. 20).

This review is now ended with a few comments.

CONCLUDING REMARKS

Four examples have been reviewed of optical measurement techniques, used at Lewis for measuring and visualizing the properties of propulsion flows. If the objective is very precise, automated, computerized measurement of three-dimensional properties, then double-exposure, diffuse-illumination, heterodyne, holographic interferometry appears to be the best choice. If the objectives for flow measurements are simplicity and low cost, then rainbow schlieren or moire deflectometry may be desirable. For one view, heterodyne moire deflectometry offers precision approaching that of heterodyne diffuse-illumination interferometry, and is capable of being automated and computerized. Time-average holography continues to be valuable for vibrational analysis of components and offers advantages for three-dimensional flow visualization.

Perhaps the most difficult question is the practicality of using a particular technique in a propulsion test facility, such as a wind tunnel. A definitive answer often requires an actual attempt.

REFERENCES

1. Shardin, H.: Schlieren Methods and Their Applications. NASA TT-F-12731, 1970. [translation from Ergeb. Exakten Naturewiss, vol. 20, 1942, pp. 303-439].

2. Howes, W.L.; and Buchele, D.R.: Optical Interferometry of Inhomogeneous Gases. J. Opt. Soc. Am., vol. 56, no. 11, 1966, pp. 1517-1528.

3. Maiman, T.H.: Stimulated Optical Radiation in Ruby. Nature, vol. 187, Aug. 6, 1960, pp. 493-494.

4. Powell, R.L.; and Stetson, K.A.: Interferometric Vibration Analysis by Wavefront Reconstruction. J. Opt. Soc. Am., vol. 55, no. 12, Dec. 1965, pp. 1593-1598.

5. Seasholtz, R.G.; and Goldman, L.J.: Laser Anemometer using a Fabry-Perot Interferometer for Measuring Mean Velocity and Turbulence Intensity Along the Optical Axis in Turbomachinery. Engineering Applications of Laser Velocimetry, H.W. Coleman and P.A. Pfund, eds., ASME, 1982, pp. 93-101.

6. Powell, J.A.; Strazisar, A.J. and Seasholtz, R.G.: Efficient Laser Anemometer for Intra-Rotor Flow Mapping in Turbomachinery. J. Eng. Power, vol. 103, no. 2, Apr. 1981 pp. 424-429.

7. Strazisar, A.J.; and Powell, J.A.: Laser Anemometer Measurements in a Transonic Axial Flow Compressor Rotor. Measurement Methods in Rotating Components of Turbomachinery, B. Lakshminarayana and P.W. Runstadler, eds., ASME, 1980, pp. 165-176.

8. Strazisar, A.J.; and Chima, R.V.; Comparison Between Optical Measurements and a Numerical Solution of the Flow Field in a Transonic Axial Flow Compressor Rotor. AIAA Paper 80-1078, June 1980.

9. Seasholtz, R.G.; and Goldman, L.J.: Three Component Velocity Measurements Using Fabry-Perot Interferometer. Second International Symposium on Applications of Laser Anemometry to Fluid Mechanics, Instituto Superior Tecnico, 1985, pp. 8.6-8.12.

10. Adamovsky, G.; and Piltch, N.D.: Fiber-Optic Thermometer using Temperature Dependent Absorption, Broadband Detection, and Time Domain Referencing. Submitted for publication in Appl. Opt., 1986.

11. Howes, W.L.: Rainbow Schlieren and its Applications. Appl. Opt., vol. 23, no. 14, July 15, 1984, pp. 2449-2460.

12. Klauminzer, G.K.: Twenty Years of Commercial Lasers-A Capsule History. Laser Focus/Electro-Optics, vol. 20, no. 12, Dec. 1984, pp. 54-79.

13. Decker, A.J.: Pulse Modulation Effect on Velocity Fringes. Appl. Opt., vol. 14, no. 5, May 1975, pp. 1061-1063.

14. Decker, A.J.: Holographic Flow Visualization of Time-Varying Shock Waves. Appl. Opt., vol. 20, no. 18, Sept. 15, 1981, pp. 3120-3127.

15. Decker, A.J.: Measurement of Fluid Properties Using Rapid-Double-Exposure and Time-Average Holographic Interferometry. AIAA Paper 84-1461, June 1984.

16. Decker, A.J.: Fringe Localization Requirements for Three-Dimensional Flow Visualization of Shock Waves in Diffuse-Illumination, Double-Pulse Holographic Interferometry. NASA TP-1868, 1982.

17. Boldman, D.R.; Buggele, A.E.; and Decker, A.J.: Three-Dimensional Shock Structure in a Transonic Flutter Cascade. AIAA J., vol. 20, no. 8, Aug. 1982, pp. 1146-1148.

18. Decker, A.J.; and Stricker, J.: A Comparison of Electronic Heterodyne Moire Deflectometry and Electronic Heterodyne Holographic Interferometry for Flow Measurements. SAE Paper 851896, 1985.

19. Crane, R.: Interference Phase Measurements. Appl. Opt. vol. 8, no. 3, Mar. 1969, pp. 538-542.

20. Dändliker, R.: Heterodyne Holographic Interferometry. Progress in Optics, vol. 17, E. Wolf, ed., North Holland, 1980, pp. 1-84.

21. Dändliker, R.; and Thalmann, R.: Hetrodyne and Quasi-heterodyne Holographic Interferometry. Opt. Eng., vol. 24, no. 5, Sept.-Oct. 1985, pp. 824-831.

22. Stricker, J.: Electronic Heterodyne Readout of Fringes in Moire Deflectometry. Opt. Lett., vol. 10, no. 6, June 1985, pp. 247-249.

23. Stricker, J.: Moire Deflectometry with Deferred Electronic Heterodyne Readout. Appl. Opt., vol. 24, no. 15, Aug. 1, 1985, pp. 2298-2299.

24. Stricker, J.: Diffraction Effects and Special Advantages in Electronic Heterodyne Moire Deflectometry. Appl. Opt., vol. 25, no. 6, Mar. 15, 1986, pp. 895-902.

25. Leith, E.N; and Upatnieks, J.: Reconstructed Wavefronts and Communication Theory. J. Opt. Soc. Am., vol. 52, no. 10, Oct. 1962, pp. 1123-1130.

26. Collier, R.J.; Burckhardt, C.B.; and Lin, L.H.: Optical Holography. Academic Press, 1971.

27. Caulfield, H.J., ed.: Handbook of Optical Holography. Academic Press, 1979.

28. Decker, A.J.: Evaluation of Diffuse-Illumination Holographic Cinematography in a Flutter Cascade. NASA TP-2593, 1986.

29. Born, M.; and Wolf, E.: Principles of Optics, 3rd ed., Pergamon Press, 1965, pp. 109-132.

30. Vest, C.M.: Holographic Interferometry. Wiley, 1979.

31. Dändliker, R.; and Eliasson, B.: Accuracy of Heterodyne Holographic Strain and Stress Determination. Exp. Mech., vol. 19, no. 3, Mar. 1979, pp. 93-101.

32. Deans, S.R.: The Radon Transform and Some of its Applications. Wiley, 1983.

33. Howes, W.L.; and Buchele, D.R.: A Theory and Method for Applying Interferometry to the Measurement of Certain Two-Dimensional Gaseous Density Fields. NACA TN-2693, 1952.

34. Goodman, J.W.: Introduction to Fourier Optics. McGraw-Hill, 1968.

35. Kafri, O.: Noncoherent Method for Mapping Phase Objects. Opt. Lett., vol. 5, no. 12, Dec. 1980, pp. 555-557.

36. Stricker, J.; and Kafri, O.: A New Method for Density Gradient Measurements in Compressible Flows. AIAA J., vol. 20, no. 6, June 1982, pp. 820-823.

37. Keren, E.; and Kafri, O.: Diffraction Effects in Moire Deflectometry. J. Opt. Soc. Am. A, vol. 2, no. 2, Feb. 1985, pp. 111-120.

38. Decker, A.J.: Holographic Cinematography of Time-Varying Reflecting and Time-Varying Phase Objects Using a Nd:YAG Laser. Opt. Lett., vol. 7, no. 3, Mar. 1982, pp. 122-123.

39. Goodman, J.W.: Statistical Properties of Laser Speckle Patterns. Laser Speckle and Related Phenomena, J.C. Dainty, ed., Springer-Verlag, 1975, pp. 9-75.

40. Wuerker, R.F., et al.: Application of Holography to Flow Visualization within Rotating Compressor Blade Row. (AIRESEARCH-73-9489, AiResearch Manufacturing Co.; NASA Contract NAS3-15336) NASA CR-121264, 1974.

41. Weimer, D.: Pockels Effect Cell for Gas-Flow Simulation. NASA TP-2007, 1982.

42. Stetson, K.A.: Effects of Beam Modulation on Fringe Loci and Localization in Time-Average Holographic Interferometry. J. Opt. Soc. Am., vol. 60, no. 10, Oct. 1970, pp. 1378-1388.

43. Wilson, A.D.: Characteristic Functions for Time-Average Holography. J. Opt. Soc. Am., vol. 60, no. 8, Aug. 1970, pp. 1068-1071.

44. Decker, A.J.: Analytical Procedure for Evaluating Speckle-Effect Instrumentation. NASA TM X-3478, 1977.

45. Howes, W.L.: Rainbow Schlieren vs Mach-Zehnder Interferometer: A Comparison. Appl. Opt., vol. 24, no. 6, Mar. 15, 1985, pp. 816-822.

46. Howes, W.L.: Rainbow Schlieren. NASA TP-2166, 1983.

47. Howes, W.L.: Large Aperture Interferometer with Local Reference Beam. Appl. Opt., vol. 23, no. 10, May 15, 1983, pp. 1467-1473.

48. Settles, G.S.: Color Schlieren Optics-A Review of Techniques and Applications. Flow Visualization, II, W. Merzkirch, ed., Hemisphere, 1982, pp. 749-762.

PERIOD	TECHNIQUE	MEASURED OR VISUALIZED PROPERTY
1943 - 1947	TÖPLER SCHLIEREN	DENSITY GRADIENT
	SHADOWGRAPHY	DENSITY SECOND DERIVATIVE
1948 - 1971	MACH-ZEHNDER INTERFEROMETRY	DENSITY
1972 - PRESENT	RAINBOW SCHLIEREN	DENSITY GRADIENT
	MOIRE DEFLECTOMETRY	DENSITY GRADIENT
	LASER INTERFEROMETRY	DENSITY
	DOUBLE - EXPOSURE, DIFFUSE - ILLUMINATION HOLOGRAPHIC INTER-FEROMETRY	DENSITY CHANGE OR GRADIENT OF DENSITY-CHANGE OR STRUCTURAL DIS-PLACEMENT
	TIME-AVERAGE HOLOGRAPHIC INTERFEROMETRY	DENSITY-CHANGE AMPLITUDE OR GRADIENT OF DENSITY-CHANGE AMPLITUDE OR STRUCTURAL-DISPLACEMENT AMPLITUDE
	SPECKLE INTERFEROMETRY	STRUCTURAL DIS-PLACEMENT

Figure 1. - History of applications of interferometry and deflectometry at NASA Lewis Research Center.
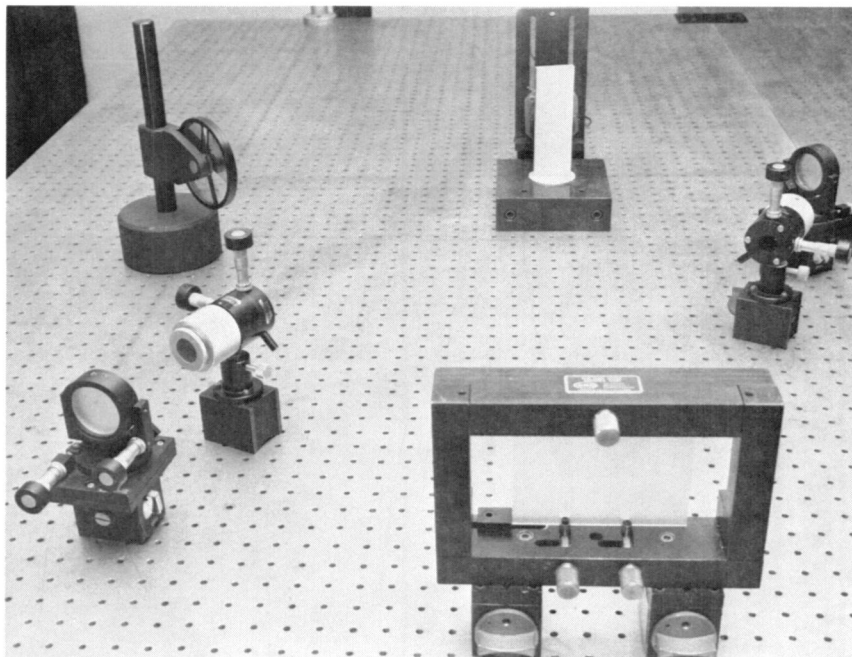
Figure 2. - Simple holography set-up.
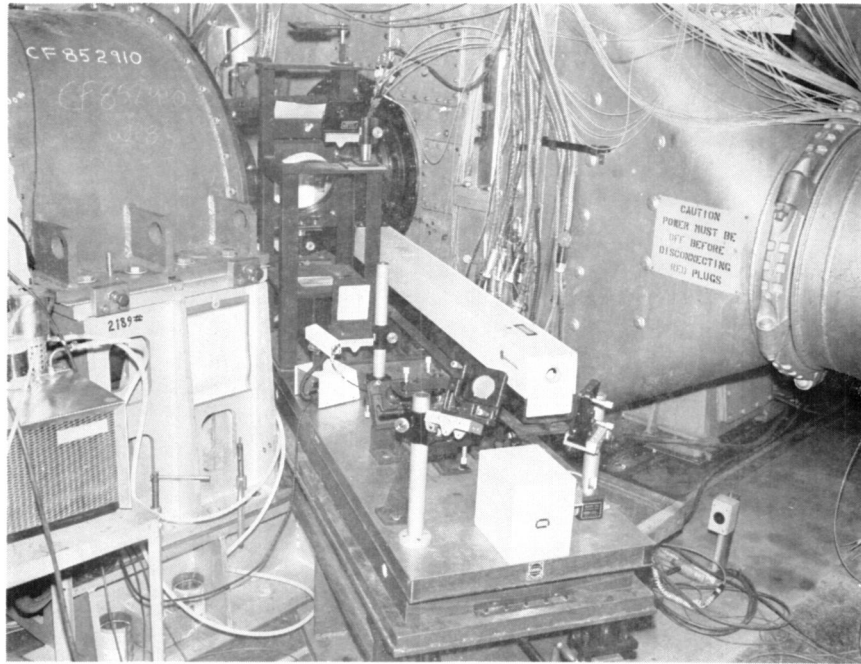
Figure 3. - Complex holography set-up in single-stage transonic compressor facility.
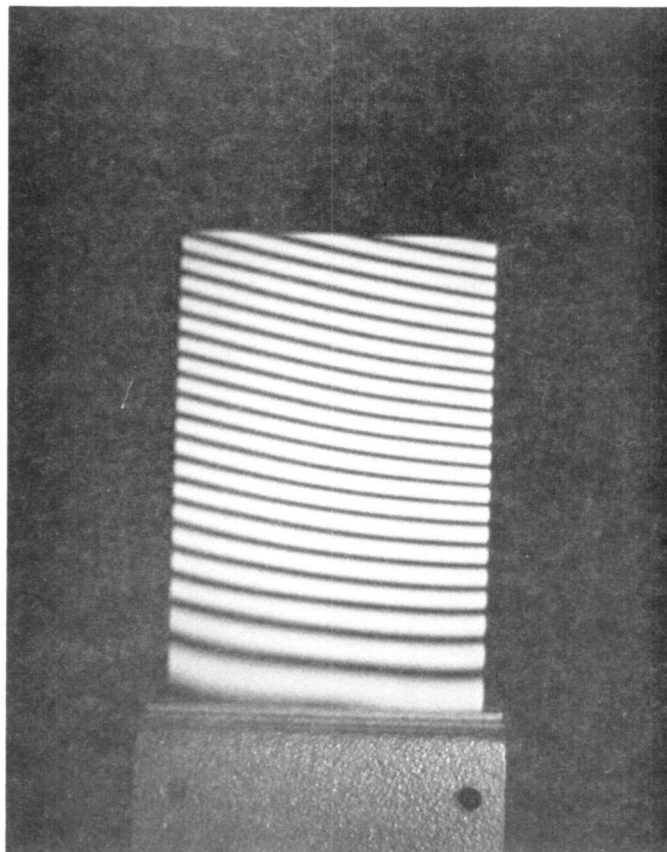
Figure 4. - Cosine interference-fringe pattern between bent and unbent states of cantilever.

STRUCTURE

$\vec{k_i}$

$\vec{\delta}$

$\vec{k_r}$

HOLOGRAM

CAMERA OF EYE

- $\vec{k_i}$ IS A UNIT VECTOR ALONG THE INCIDENT LIGHT RAY

- $\vec{k_r}$ IS A UNIT VECTOR ALONG THE REFLECTED LIGHT RAY

- $\vec{\delta}$ IS STRUCTURAL DISPLACEMENT AT REFLECTION POINT OF LIGHT RAY
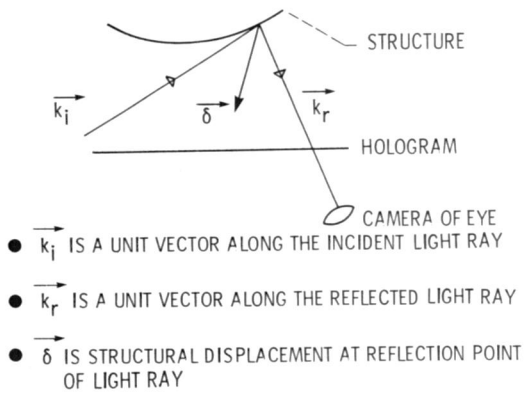
Figure 5. - Geometry for computing change of phase of light ray due to displacement of structure.

ORIGINIAL DIRECTION OF INCIDENT LIGHT

Y

X

Z

DIFFUSER

APPARENT POSITION OF FRINGE PATTERN $\partial \Delta \Phi / \partial \theta_{ix} = 0$

HOLOGRAM

LIGHT RAY i

LENS OR IMAGING SYSTEM
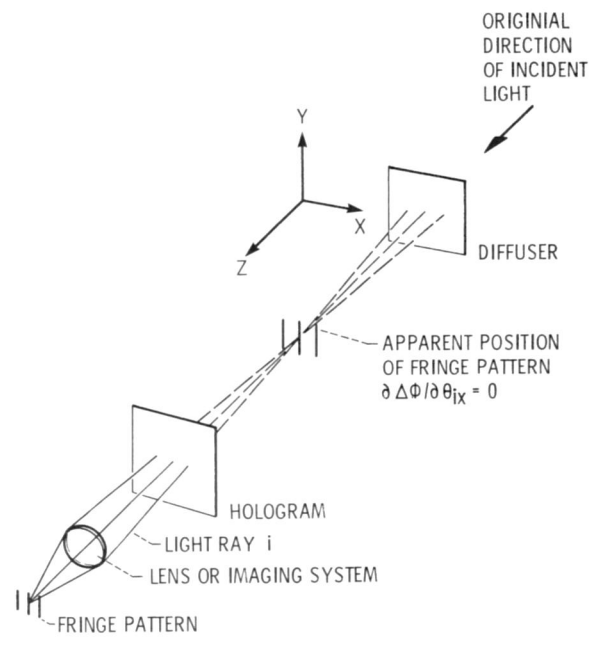
FRINGE PATTERN

Figure 6 - Imaging a localized interference fringe pattern.

FRINGE LOCALIZATION
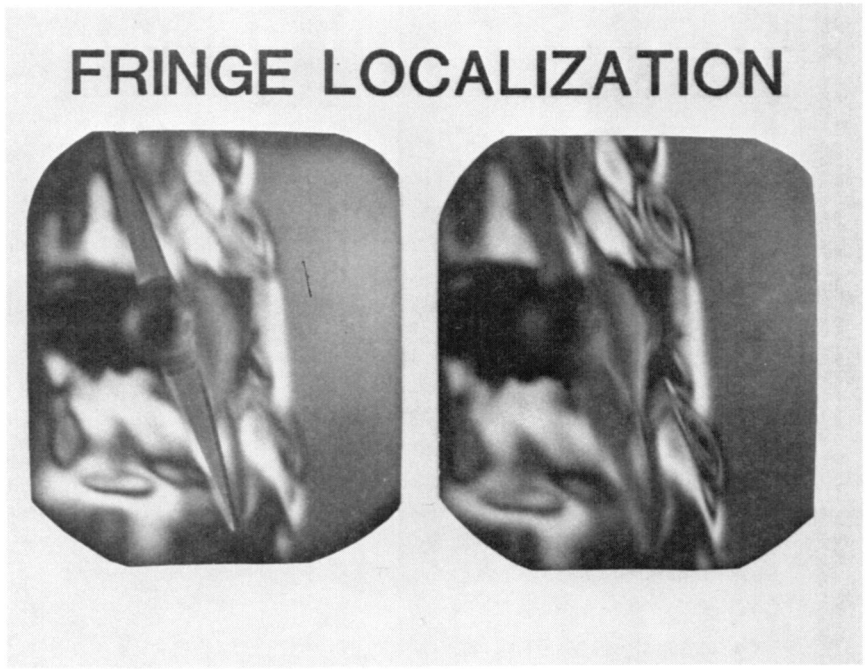
Figure 7. - Fringe localization for flame induced flow. Camera focused on reconstruction o blade tip in left photograph and for maximum fringe contrast in right photograph.

Angle 1

Angle 2

⌐Typical
shock
wave

Angle 3

⌐Typical
shock
wave

An_e 4
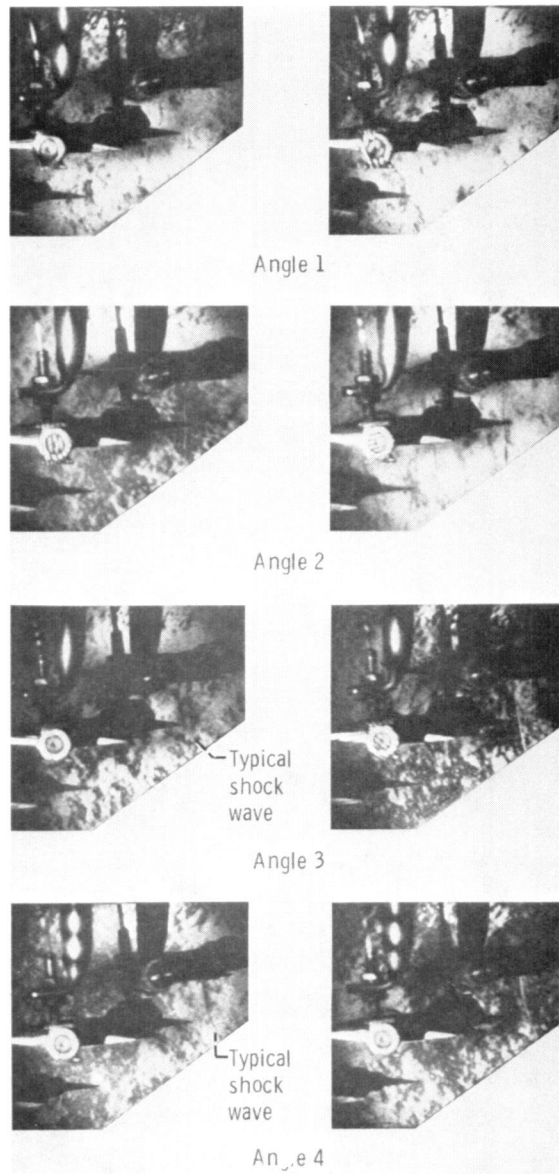
Figure 8. - Reconstructed images from holograms of shock
structure in three-blade flutter cascade.
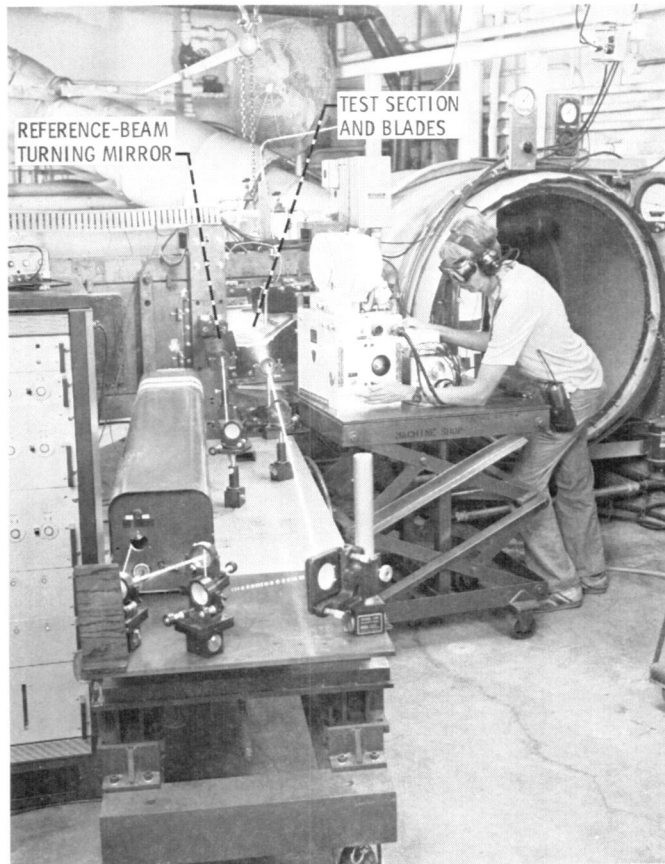
Figure 9. - Holography set-up in three-blade flutter cascade.
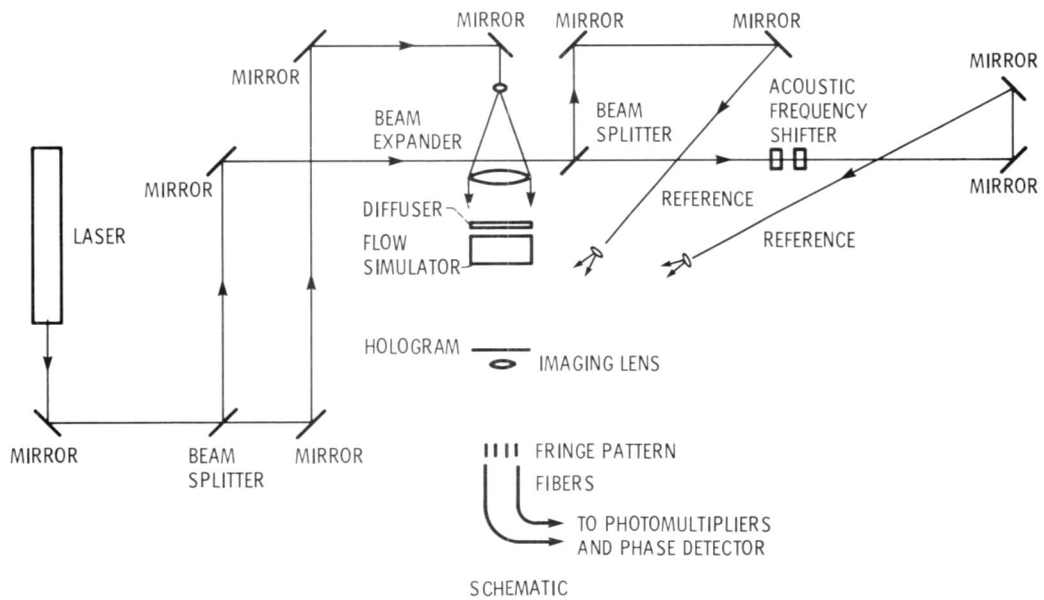
Figure 10. - Setup for double-exposure, diffuse-illumination, heterodyne, holographic interferometry.

INCIDENT LIGHT

PLANE OF POLARIZATION

TO H. V.

#1

5 cm

#4

5 cm

3 cm

#2

y

#3

TO H.V.

x

z
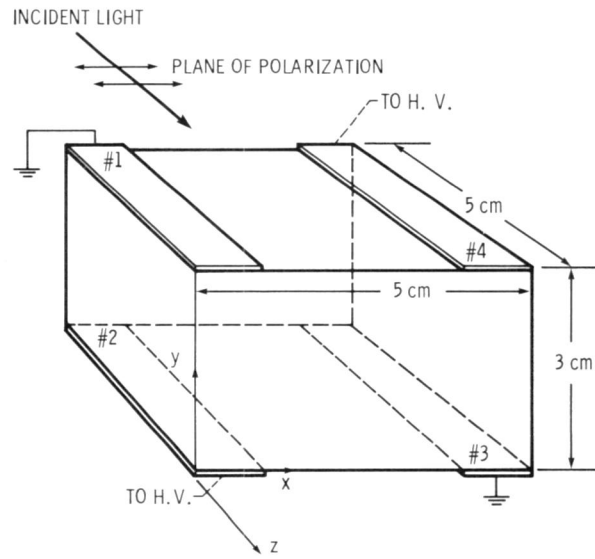
FLOW SIMULATOR-CRYSTAL OF KD*P

Figure 11. - Flow simulator.

Electrode 1   Electrode 4

Electrode 2   Electrode 3

(a) Potential of 7 kV.   (b) Potential of 6kV.

(c) Potential of 5 kV.   (d) Potential of 4kV.

(e) Potential of 3 kV.   (f) Potential of 2kV.
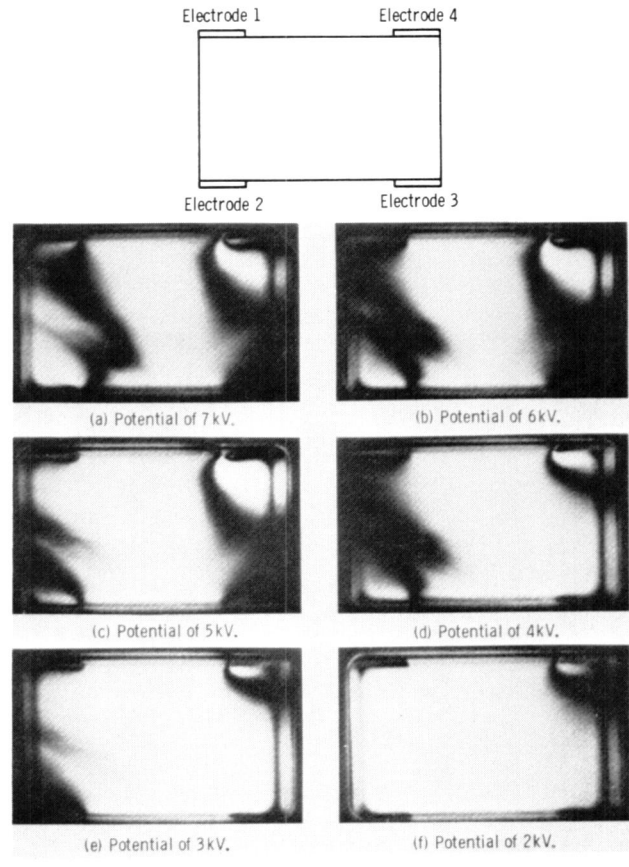
Figure 12. - Interferograms for flow simulator.

ERROR   1/50   1/100   1/300   1/600   FRINGE

EXPECTED SCATTER FROM
RANDOM ERRORS ILLUSTRATED
FOR COMPARISON WITH DATA
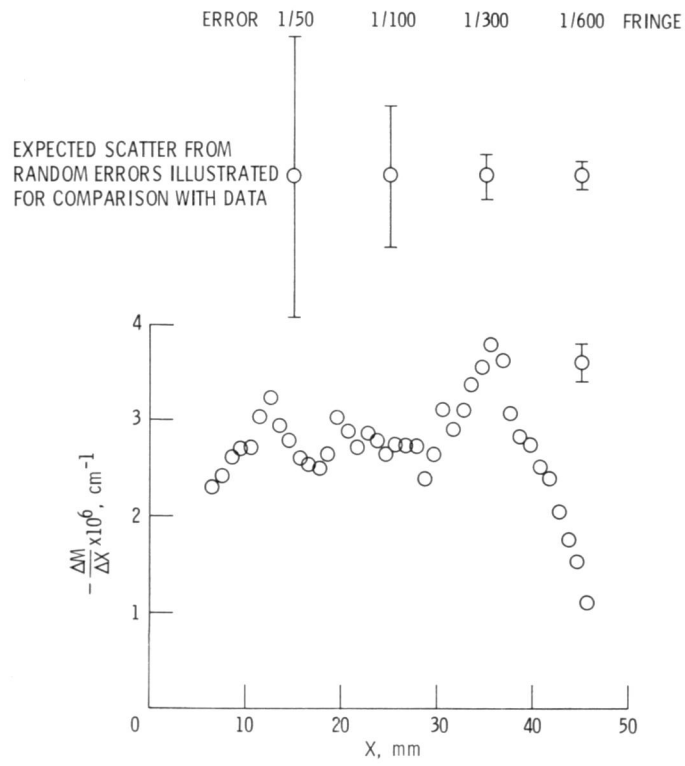
Figure 13. – Result for heterodyne measurement of 5 KV condition of flow
simulator.

0 HZ.

855 HZ.
1st BENDING

2047 HZ.
1st TORSIONAL

5441 HZ.
2nd BENDING

6569 HZ.
LYRE

7359 HZ.
2nd TORSIONAL
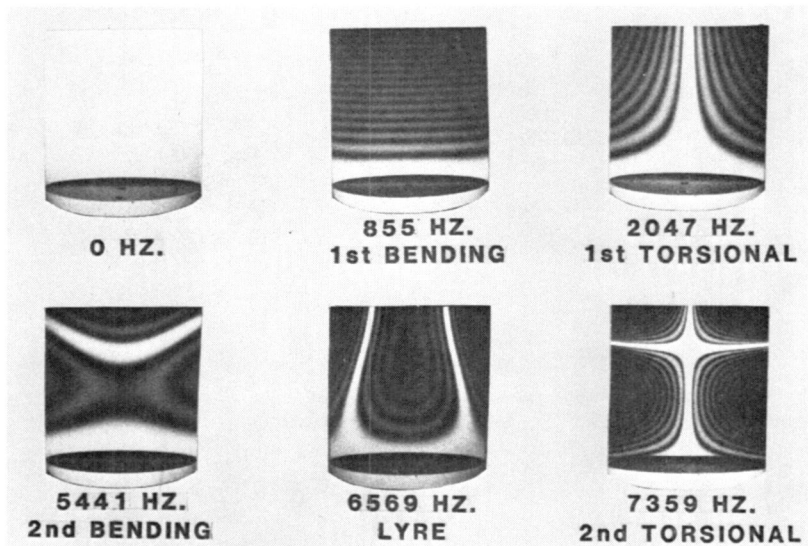
Figure 14. – Mode shapes of blade.
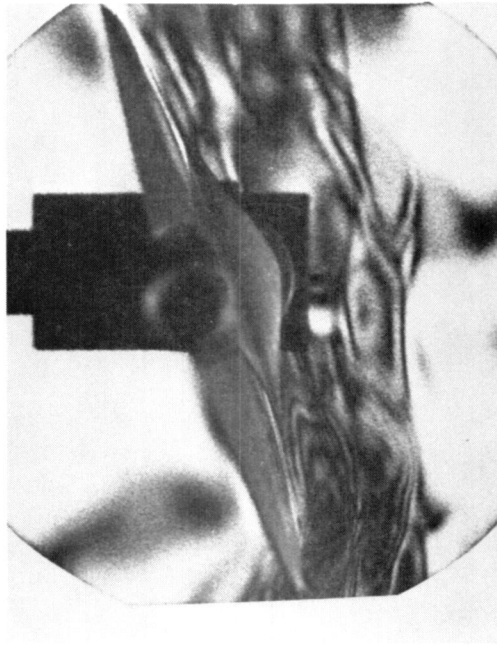
Figure 15. - Time- average fringe pattern for flame-
induced flow over blade.
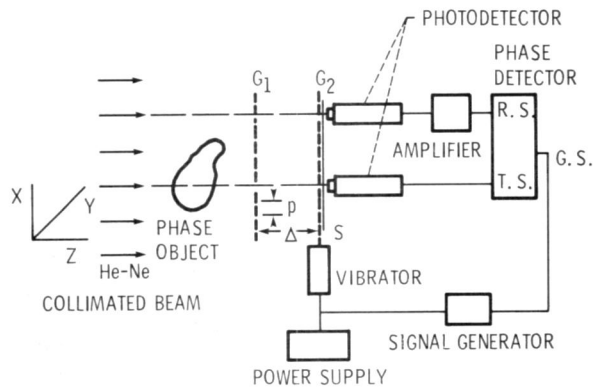
(a) Schematic of moire deflectometer with electronic heterodyne readout.
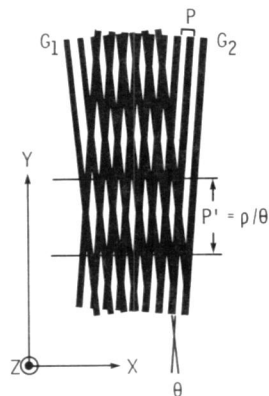
(b) Moire fringe pattern formed by Ronchi gratings.

Figure 16. - Moire deflectometry.
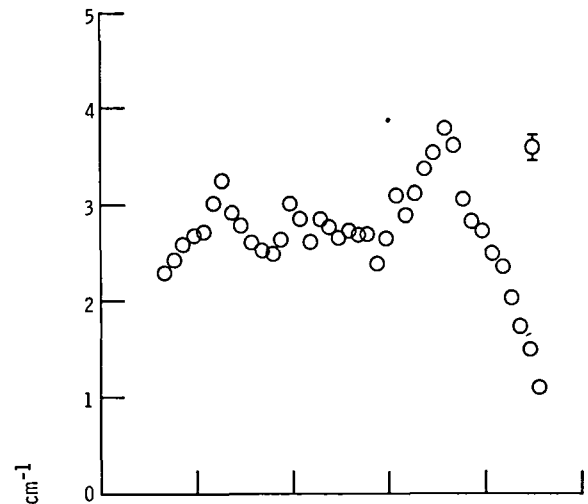
(a) Heterodyne holography.
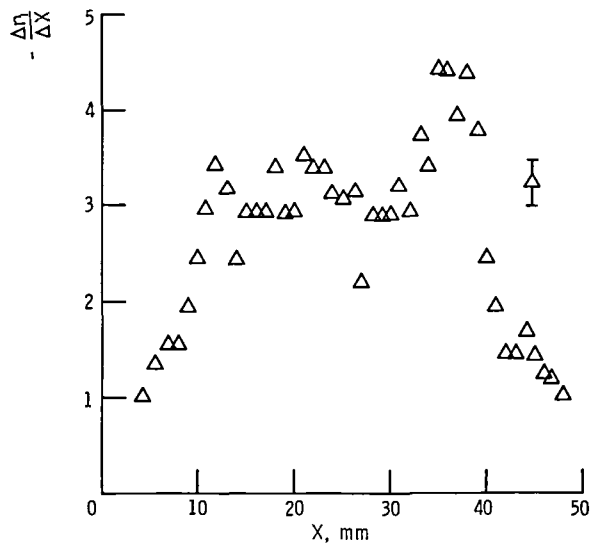
(b) Heterodyne moire.

Figure 17. - Comparison of heterodyne holographic inter-
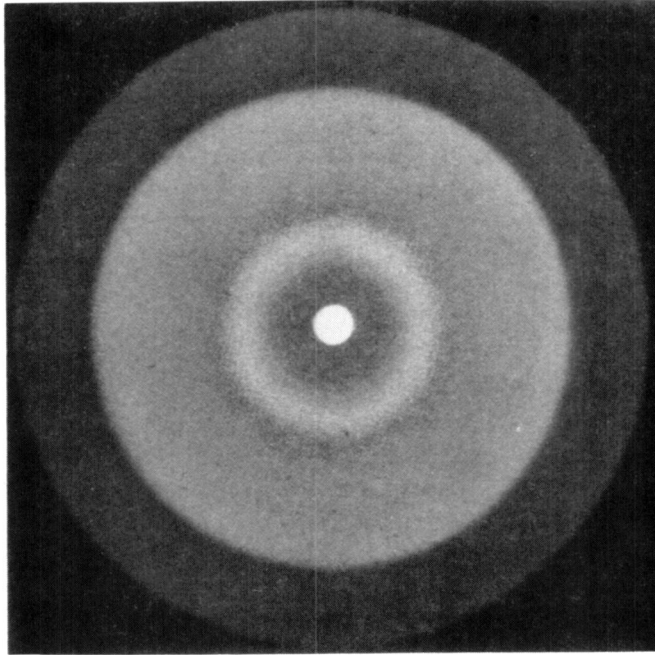ferometry with heterodyne moire deflectometry.
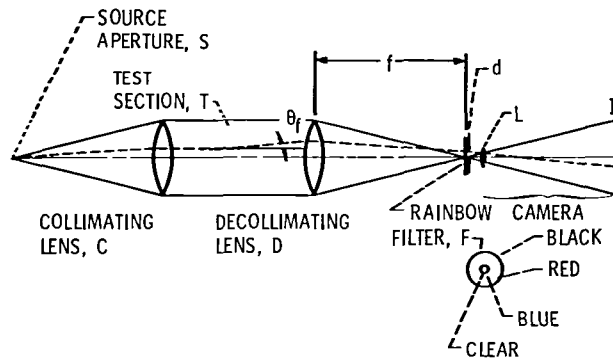
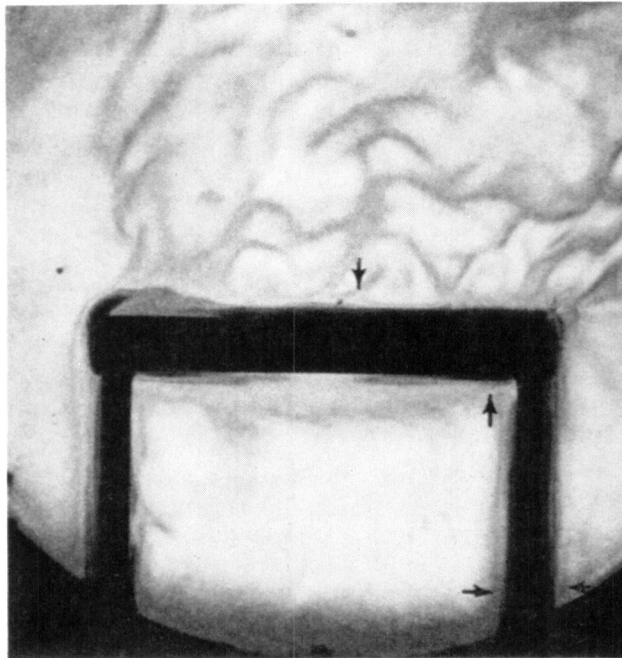
Figure 18. - Rainbow schlieren.

Figure 19. - Photographic enlargement of rainbow filter.
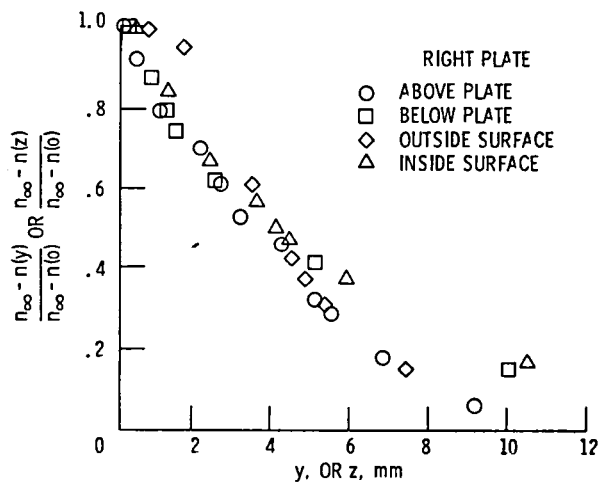

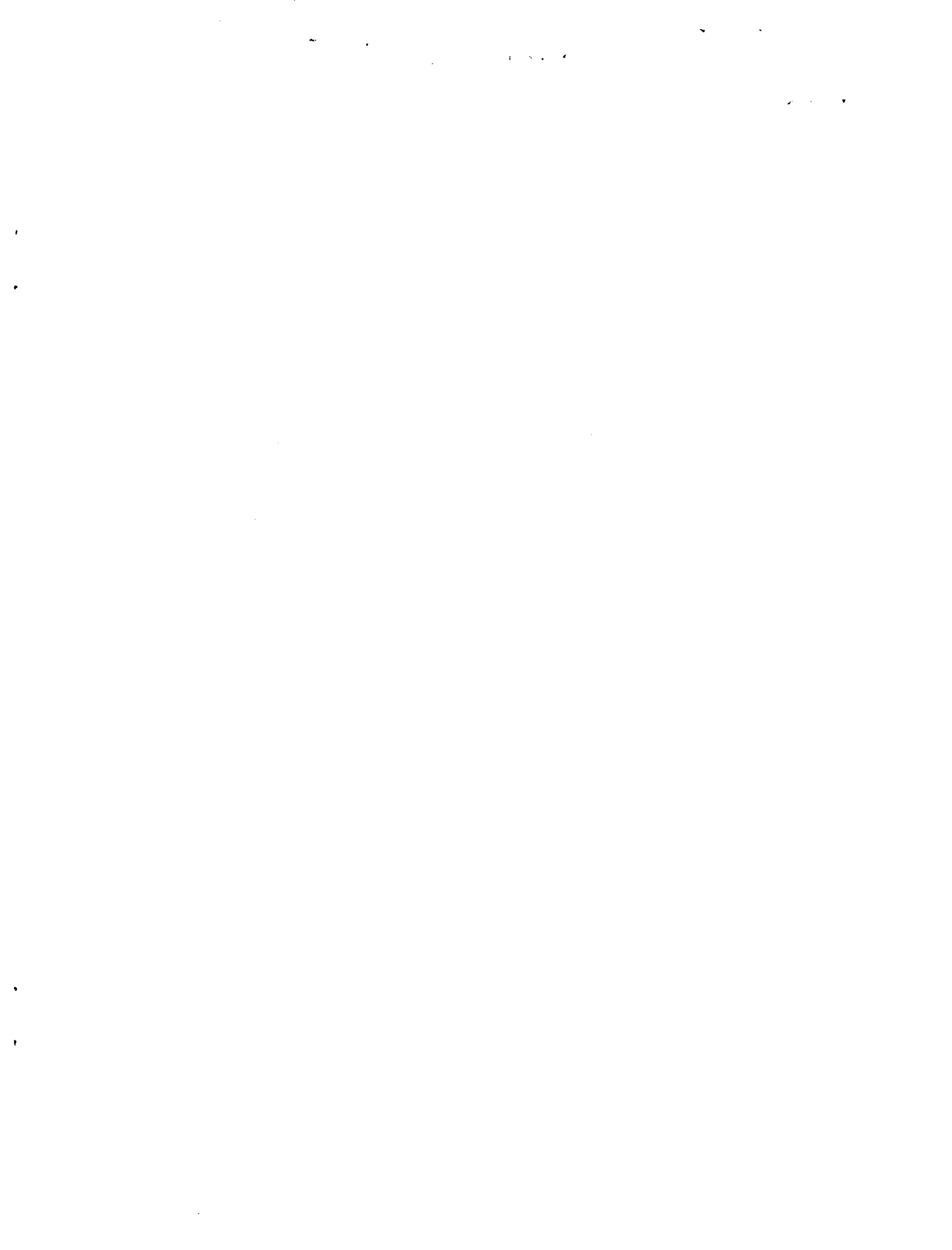Figure 20. - Refraction field around heated flat plates.

Figure 21.- Refractive index distribution near horizontal and vertical plates.

1. Report No. NASA TM-88829	2. Government Accession No.	3. Recipient's Catalog No.

4. Title and Subtitle	5. Report Date
Advanced Optical Measuring Systems for Measuring the Properties of Fluids and Structures	
	6. Performing Organization Code 505-62-01

7. Author(s)	8. Performing Organization Report No.
Arthur J. Decker	E-3204
	10. Work Unit No.

9. Performing Organization Name and Address	11. Contract or Grant No.
National Aeronautics and Space Administration Lewis Research Center Cleveland, Ohio 44135	
	13. Type of Report and Period Covered

12. Sponsoring Agency Name and Address	Technical Memorandum
National Aeronautics and Space Administration Washington, D.C. 20546	14. Sponsoring Agency Code

15. Supplementary Notes

16. Abstract

Four advanced optical methods are reviewed for the measurement or visualization of flow and structural properties. Double-exposure, diffuse-illumination, holographic interferometry can be used for three-dimensional flow visualization. When this method is combined with optical heterodyning, precise measurements of structural displacements or fluid density are possible. Time-average holography is well known as a method for displaying vibrational mode shapes, but it also can be used for flow visualization and flow measurements. Deflectometry is used to measure or visualize the deflection of light rays from collimation. Said deflection occurs because of refraction in a fluid or because of reflection from a tilted surface. The moire technique for deflectometry, when combined with optical heterodyning, permits very precise measurements of these quantities. The rainbow schlieren method of deflectometry allows varying deflection angles to be encoded with colors for visualization.

17. Key Words (Suggested by Author(s))	18. Distribution Statement
Holographic interferometry; Flow visualization; Schlieren photography; Moire effects; China (Mainland); Optical measuring instruments	Unclassified - unlimited STAR Category 35

19. Security Classif. (of this report)	20. Security Classif. (of this page)	21. No. of pages	22. Price*
Unclassified	Unclassified		

National Aeronautics and
Space Administration

Lewis Research Center
Cleveland, Ohio 44135

Official Business
Penalty for Private Use $300

NASA